Available online at www.sciencedirect.com
ScienceDirect
Trans. Nonferrous Met. Soc. China 24(2014) 1414−1424
Transactions of Nonferrous Metals Society of China
www.tnmsc.cn

Supercritical-hydrothermal accelerated solid state reaction route for synthesis of $LiMn_2O_4$ cathode material for high-power Li-ion batteries

Xue-wu LIU[1, 2], Jie TANG[1], Xu-song QIN[2], Yuan-fu DENG[3], Guo-hua CHEN[2, 4]

1. School of Chemical Machinery, Dalian University of Technology, Dalian 116024, China;
2. Center for Green Products and Processing Technologies, Guangzhou HKUST Fok Ying Tung Research Institute, Guangzhou 511458, China;
3. School of Chemistry and Chemical Engineering, South China University of Technology, Guangzhou 510640, China;
4. Department of Chemical and Biomolecular Engineering, Hong Kong University of Science and Technology, Clear Water Bay, Kowloon, Hong Kong, China

Received 8 May 2013; accepted 3 March 2014

Abstract: Synthesis of the spinel structure lithium manganese oxide ($LiMn_2O_4$) by supercritical hydrothermal (SH) accelerated solid state reaction (SSR) route was studied. The impacts of the reaction pressure, reaction temperature and reaction time of SH route, and the calcination temperature of SSR route on the purity, particle morphology and electrochemical properties of the prepared $LiMn_2O_4$ materials were studied. The experimental results show that after 15 min reaction in SH route at 400 °C and 30 MPa, the reaction time of SSR could be significantly decreased, e.g. down to 3 h with the formation temperature of 800 °C, compared with the conventional solid state reaction method. The prepared $LiMn_2O_4$ material exhibits good crystallinity, uniform size distribution and good electrochemical performance, and has an initial specific capacity of 120 mA·h/g at a rate of 0.1*C* (1*C*=148 mA/g) and a good rate capability at high rates, even up to 50*C*.

Key words: lithium ion battery; $LiMn_2O_4$; supercritical water; solid state reaction; high rate capability

1 Introduction

Spinel structure $LiMn_2O_4$ has received considerable attention in recent years as a cathode material for lithium ion batteries, for its excellence on the safety, cost-effectiveness and eco-friendliness compared with the conventional $LiCoO_2$ [1]. However, the application of the spinel structure $LiMn_2O_4$ is hampered by the capacity fading during cycling process due to the dissolution of Mn^{3+} ions into the electrolyte and the Jahn−Teller distortion [2]. The electrochemical properties of $LiMn_2O_4$ are intimately related to its phase purity, crystallinity, particle size and morphology [3]. All these physical and electrochemical properties of $LiMn_2O_4$ material are determined by the synthetic routes and the associated synthesis conditions. The solid state reaction method first developed by HUNTER [4] is the most popular method for $LiMn_2O_4$ synthesis. However, it has difficulties in the control of the growth rate of crystals, morphology and particle size distribution. It also requires excessive calcination time at high temperature, e.g. 72 h at 800 °C as reported by GUYOMARD and TARASCON [5]. Moreover, it suffers from the phase impurity problem, which may lead to significant losses in the specific capacity and the cycling stability of the prepared $LiMn_2O_4$. In order to overcome these disadvantages, various techniques are developed, such as spray-drying [6], sol−gel [7], micro-wave [8], micro-emulsion [9] and spray pyrolysis [10] methods. However, these methods have some drawbacks such as expensive raw materials and complicated preparation processes required, making these synthesis methods not appropriate for large-scale $LiMn_2O_4$ production.

Recently, supercritical water has received significant attention as a new reaction medium for the

Foundation item: Project supported by the Research Funds of the Key Laboratory of Fuel Cell Technology of Guangdong Province, China; Project (7411793079907) supported by the Guangzhou Special Foundation for Applied Basic Research; Project (2013A15GX048) supported by the Dalian Science and Technology Project Foundation, China; Project (21376035) supported by the National Natural Science Foundation of China

Corresponding author: Xue-wu LIU; Tel/Fax: +86-411-84986276; E-mail: liuxuewu@dlut.edu.cn

DOI: 10.1016/S1003-6326(14)63207-6

synthesis of nanoparticles due to its unique properties of low viscosity, high diffusivity, zero surface tension, and nontoxicity. Various high quality and highly crystallized nano-sized particles have been synthesized in supercritical water, such as Fe_3O_4 [11], Zn_2SnO_4 [12], $LiFePO_4$ [13], $LiFePO_4$/C [14], $LiMn_2O_4$ [15] and $Li_4Ti_5O_{12}$ [16]. However, it is worth to point out that because the reaction time for the synthesis of the nano-sized particles in supercritical water is short, typically not longer than 15 min [13,15,16], the phase impurity and poor crystallinity problems might happen. A subsequent heat-treatment is therefore required to remove the impure particles and improve the crystallinity of the particles. Therefore, the synthesis conditions of supercritical hydrothermal process and the subsequent solid state reaction play an important role in the morphology, particle size and crystallinity of the final products as well as the electrochemical properties.

In this study, spinel structure $LiMn_2O_4$ cathode material was synthesized by the SH accelerated SSR route. The impacts of the reaction pressure, reaction temperature and reaction time of SH route, and the calcination temperature of SSR route on the purity, particle morphology and electrochemical properties of the prepared $LiMn_2O_4$ material were studied using one-factor-at-a-time experimental method.

2 Experimental

2.1 Chemicals

$Mn(NO_3)_2$ (50%, mass fraction; Guangzhou Chemical Reagent, China) and $LiOH·H_2O$ (98%, Sigma-Aldrich, USA) were used as-received as the reactants for the synthesis of $LiMn_2O_4$ cathode material in this study. Deionized water of a resistivity as 18 MΩ·cm produced by a deionized water production system (Model BRAIT-HiDi-10, Shanghai Baolor, China) was used to prepare the LiOH and $Mn(NO_3)_2$ solutions. Concentrated $NH_3·H_2O$ solution (25%, Guangzhou Chemical Reagent, China) was used to adjust the pH of the mixture solution.

2.2 Apparatuses and procedures

In this study, a supercritical hydrothermal batch reactor and a high temperature furnace (Model RHF 1400, Carbolite Limited, England) were used to synthesize the $LiMn_2O_4$ particles. The schematic diagram of the supercritical hydrothermal batch reactor is shown in Fig. 1. It mainly consists of a temperature control system (including a high temperature furnace, a temperature transmitter and a temperature controller), a reaction kettle equipped with a water jacket, a cooling system (including a cooling water tank and a magnetic pump) and a pressure control system (including a pressure transmitter, a pressure release valve and a pressure controller). A brief description of the synthesis procedures of $LiMn_2O_4$ by the SH accelerated SSR route is given below.

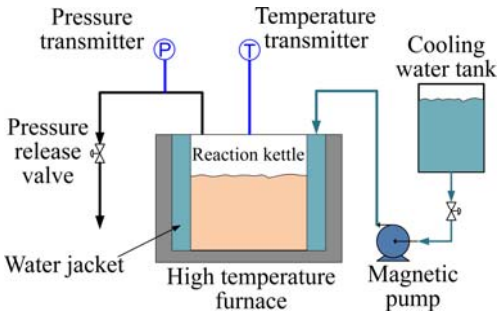

Fig. 1 Schematic diagram of supercritical hydrothermal batch reactor

The reactants, $LiOH·H_2O$ and $Mn(NO_3)_2$, were dissolved in deionized water individually with the corresponding concentrations of 0.2174 and 0.0266 mol/L, respectively. A mixture was then prepared by mixing 50 mL LiOH solution and 100 mL $Mn(NO_3)_2$ solution according to the molar ratio required, namely, n(Li):n(Mn)=4:1. The concentrated $NH_3·H_2O$ solution was then added to adjust the pH of the mixture, and deionized water was added to make 200 mL mixture. As the consequence, the pH of the mixture solution was 10.7, and the concentrations of LiOH and $Mn(NO_3)_2$ in the mixture solution were 0.054 and 0.0134 mol/L, respectively. The prepared mixture solution was then transferred to the reaction kettle, and placed inside of the high temperature furnace which had been preheated to the specified temperature of each experimental run. The temperature of the furnace was controlled by a temperature controller to keep the reaction temperature of the mixture at specified temperatures. At the same time, the pressure release value was manipulated by another controller to maintain the reaction pressure of the mixture at specified values. During the reaction, the reaction pressure and temperature of SH route were also monitored by a pressure gauge and a thermometer respectively. After the specified reaction time, the high temperature furnace was shut down, and the cooling water was injected to the water jacket by the magnetic pump to cool the reaction kettle down to the room temperature. Products were then filtered and washed with deionized water. After that they were put into an oven and dried at 100 °C in air for overnight. The dried particles were finely ground and finally calcined for 3 h at the specified temperatures in the high temperature furnace (Model RHF 1400, Carbolite Limited, England).

2.3 Sample characterization

The crystalline properties of the $LiMn_2O_4$ samples were analyzed by X-ray diffraction (XRD) conducted by an X-ray diffraction system (Bruker D8 Advance, Germany) with a primary target of Cu K_α (wavelength of 1.5406 Å). The X-ray power was 1.6 kW and the diffractograms were recorded with a 2θ range of 10° to 70° at a scan speed of 0.2 (°)/s. The surface morphology of the $LiMn_2O_4$ samples was examined by scanning electron microscopy (SEM, JSM−6300F, JEOL, Japan). The samples were mounted on a circular copper holder by conductive carbon adhesion. The acceleration voltage was set as 20 or 25 kV, as shown in the SEM images.

2.4 Electrochemical measurements

A slurry consisting of the prepared $LiMn_2O_4$ powders as active material, acetylene black as conducting agent, and polyvinylidene fluoride as binder with a mass ratio of 80:10:10 in N-methyl-2-pyrolidinone was prepared. The slurry was coated onto an aluminum foil with 10 mm in diameter. After coating, the electrodes were dried at 100 °C for 3 h, and then pressed under 15 MPa. Before battery assembling, the pressed electrodes were dried overnight at 100 °C. Batteries were assembled in a glove box (the MBRAUN UNIlab glovebox workstation, M. Braun Inertgas-Systeme GmbH, Germany) in argon atmosphere using the pressed electrodes as the cathode, Celgard 2500 as separator, 1 mol/L $LiPF_6$ in ethylene carbonate/ethylmethyl carbonate (volume ratio of 3:7) as electrolyte, and the metallic lithium sheets as anode. The cells were evaluated using a commercial multichannel battery testing system (Model CT-3008W, Shenzhen Neware electronic Co. Ltd., China), and the charge/discharge voltage window was set from 3.2 to 4.4 V vs Li/Li^+ at different rates.

3 Results and discussion

3.1 Effects of SH reaction pressure on properties of LiM_2O_4 cathode material

In order to evaluate the effect of the SH reaction pressure on the physical and electrochemical properties of the $LiMn_2O_4$ particles, four samples were prepared at 25, 28, 30 and 35 MPa, respectively, with the SH reaction temperature of 400 °C and reaction time of 15 min, and followed by SSR at 800 °C for 3 h. Despite the peak intensity differences, the XRD patterns of the samples prepared at 25, 28 and 30 MPa were quite similar and no impurity phase was found in Fig. 2. However, it is worth to point out that the peak intensities of the samples are strongly related to the SH reaction pressure. Higher pressure leads to higher XRD peak intensity and higher crystallinity of the final $LiMn_2O_4$ particles. This can be explained by the unique property of supercritical water that the increase of the SH reaction pressure decreases the crystallization velocity of $LiMn_2O_4$ particles at the same SH reaction temperature. Therefore, the crystal growth rate will be lower, which results in better crystallinity of the $LiMn_2O_4$ particles. However, when the $LiMn_2O_4$ particles were prepared at a SH reaction pressure higher than 30 MPa. For example, at 35 MPa in this study, small amount of Mn_3O_4 appears, as shown in Fig. 2. The impurity phases caused by Mn_3O_4 can be attributed to the fact that the excessive pressure may hinder the embeddability of lithium ions into the Mn−O lattice.

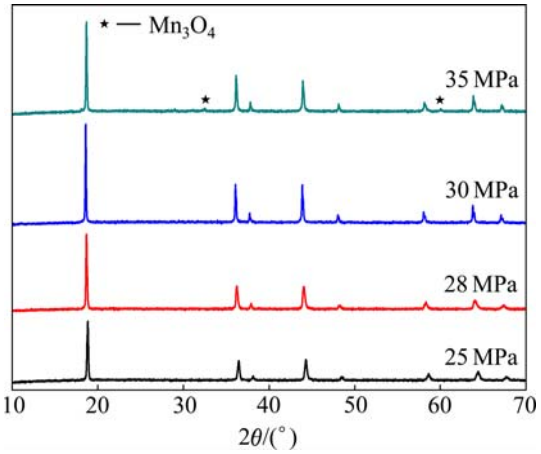

Fig. 2 XRD patterns of samples prepared at different SH reaction pressures

The SEM images of the $LiMn_2O_4$ particles are shown in Fig. 3. The particle sizes of these four samples are about 250, 250, 300 and 400 nm, respectively. Their corresponding particle size distributions are narrow. No obvious differences in morphology can be found in Fig. 3. However, as the SH reaction pressure increases, the particle size of the spinel $LiMn_2O_4$ powders increases slightly. This can be explained by the facts that in the supercritical hydrothermal process the solubility of $LiMn_2O_4$ increases with the pressure, preventing the nucleation of the new particles, and the existing fine particles are more likely to grow up and form large particles.

Electrochemical tests are performed on various samples prepared at different SH reaction pressures, as shown in Fig. 4. As seen in Fig. 4(a), for the samples prepared at higher SH reaction pressures, such as 28, 30 and 35 MPa in this study, the characteristic two voltage plateaus of $LiMn_2O_4$ at around 4.0 V can be found. However, there is no voltage plateau found for the sample prepared at SH reaction pressure of 25 MPa. Moreover, its specific capacity is only 69 mA·h/g. This value is much smaller than the specific capacities of the samples prepared at 28, 30 and 35 MPa, which are 105,

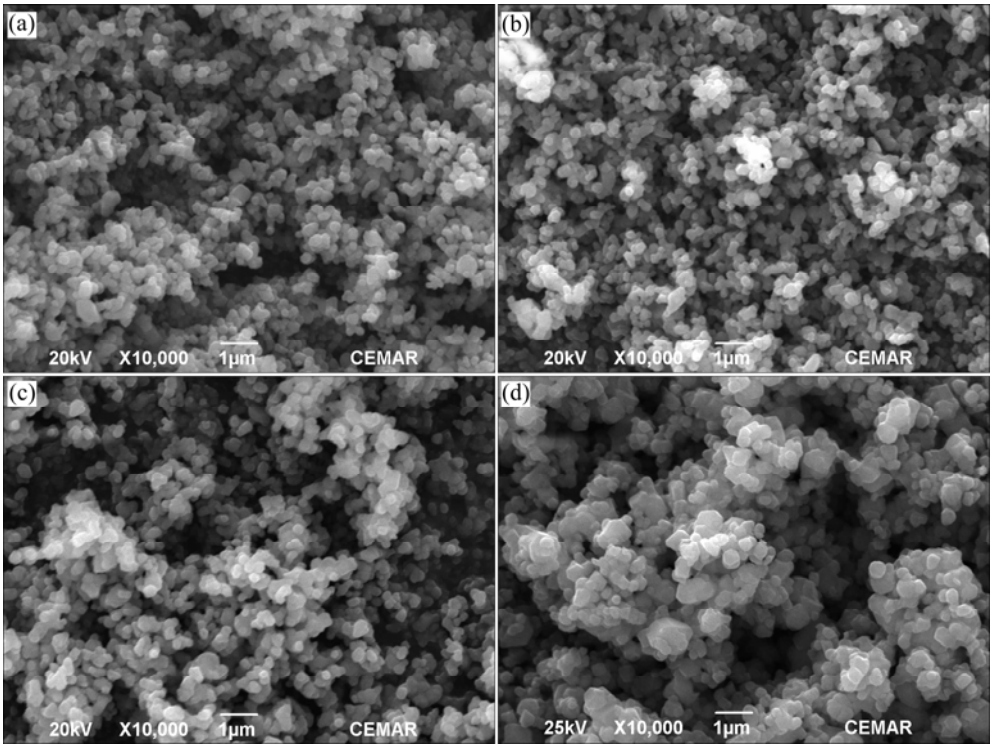

Fig. 3 SEM images of $LiMn_2O_4$ prepared at different SH reaction pressures: (a) 25 MPa; (b) 28 MPa; (c) 30 MPa; (d) 35 MPa

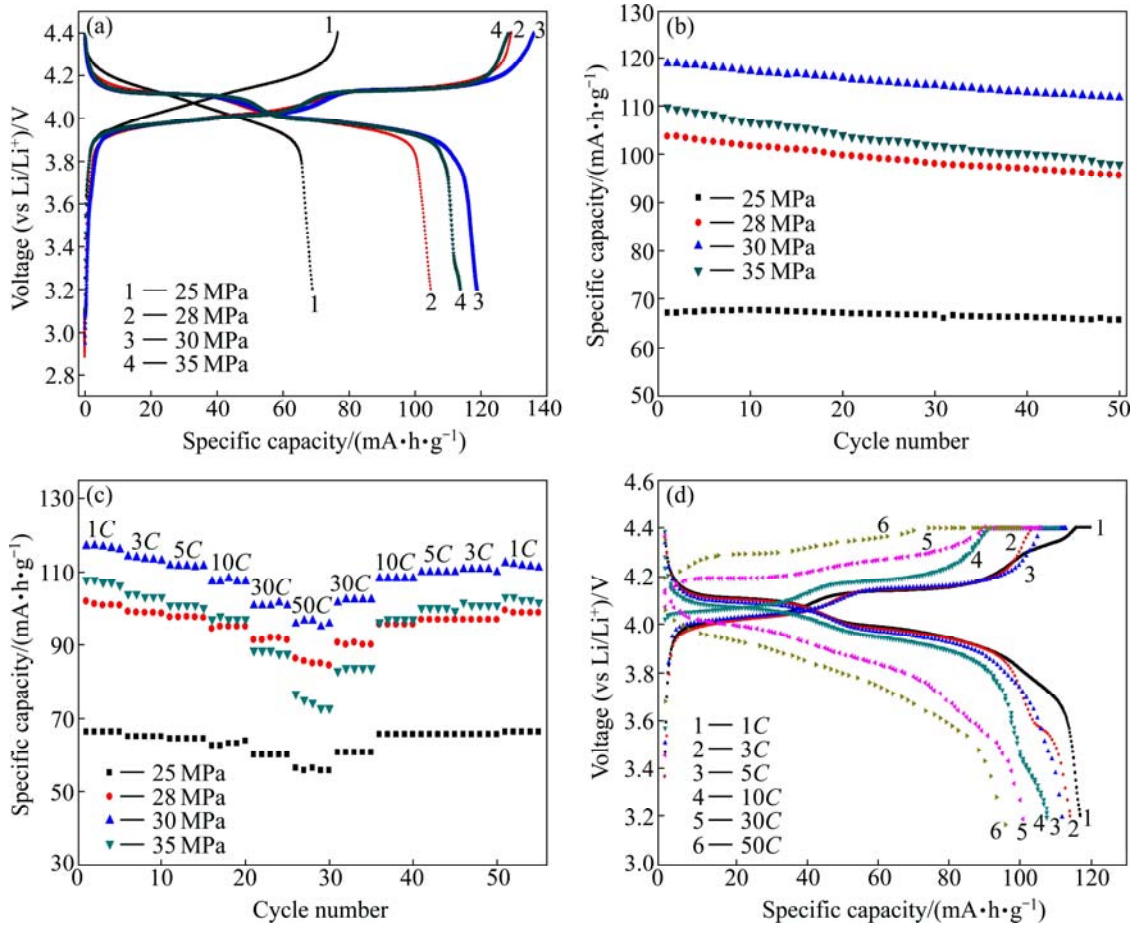

Fig. 4 Discharge−charge profiles at 0.1*C* (a), cycling performance at 1*C* (b), rate performance (c) of $LiMn_2O_4$ prepared at different SH reaction pressures and representative discharge−charge curves at different rates (d)

120 and 112 mA·h/g, respectively. This can be explained by the fact that the sample prepared at a SH reaction pressure of 25 MPa is of poor crystallinity since its peak intensities in XRD pattern are much lower compared with the other three samples, as shown in Fig. 2. In terms of cycling and rate performance, the samples prepared at a SH reaction pressure of 30 MPa maintains 96.0% of the initial capacities after 50 cycles and delivers over 95 mA·h/g of specific capacity at 50*C*, which are better than the samples prepared at 25, 28 and 35 MPa. In addition, the two characteristic voltage plateaus of $LiMn_2O_4$ at around 4.0 V can also be found for the sample prepared at 30 MPa even at a rate of 10*C*. These results are quite impressed and can be attributed to the excellent crystallinity, purity and narrow particle size distribution of the sample prepared at 30 MPa, as discussed above. As the result, the SH reaction pressure is set as 30 MPa in the following experiments.

3.2 Effects of SH reaction temperature on properties of $LiMn_2O_4$ cathode material

Four $LiMn_2O_4$ samples were prepared at 380, 390, 400 and 420 °C in SH reaction temperature, respectively, with the SH reaction pressure of 30 MPa and reaction time of 15 min, and followed by SSR at 800 °C for 3 h. Figure 5 shows the XRD patterns of the prepared $LiMn_2O_4$ samples. For the samples prepared at 380 and 390 °C, several XRD peaks which correspond to Mn_3O_4 are found. On the contrary, no impurity phase is found in the XRD patterns of the samples prepared at higher SH reaction temperatures. This means that the SH reaction temperature has a significant impact on the formation of $LiMn_2O_4$ particles. Low SH reaction temperature may lead to insufficient reactions between LiOH and $Mn(NO_3)_2$. As the consequence, the unreacted $Mn(NO_3)_2$ is then oxidized as manganese oxides, and finally Mn_3O_4 is formed in the following calcination process in the SSR route at high temperature, as shown in Fig. 5.

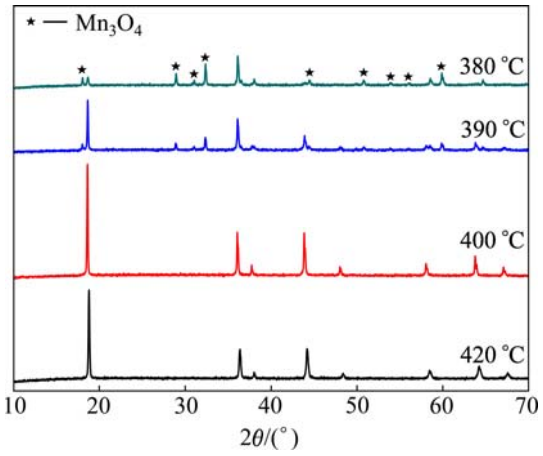

Fig. 5 XRD patterns of samples prepared at different SH reaction temperatures

Figure 6 shows the morphologies of the samples prepared at the investigated SH reaction temperatures. The morphologies of the four samples are similar. However, the crystallinity and particle size of the prepared samples vary with the SH reaction temperatures. The sample prepared at 380 °C has smallest particles. But these small particles are seriously agglomerated together, resulting in lots of amorphous blocks and lowest XRD peak intensities compared with other three samples, as shown in Fig. 5. It should be noted that the crystallinity and particle size of the sample prepared at 400 °C are better and larger, compared with those at 420, 390 and 380 °C, respectively. One of the reasons is that the reaction time of SH route and SSR route is short compared with the conventional hydrothermal synthesis method and solid state reaction method. As described above, low SH reaction temperature may lead to insufficient reactions between LiOH and $Mn(NO_3)_2$. Therefore, the subsequent SSR route only has minor impacts on the improvement of the crystallinity and the particle size of the $LiMn_2O_4$ particles. Furthermore, the viscosity of the water drops as the temperature exceeds the critical temperature. According to Walden-type equation, the diffusivity of the species of interest, e.g. Li^+ and Mn^{2+} in this study, increases correspondingly. The mass transport-controlled reaction rate is then increased, resulting in faster nucleation of $LiMn_2O_4$ particles compared with low SH reaction temperature. Thus, the size of the particles is smaller due to the quick exhaustion of the interested species, e.g. the $LiMn_2O_4$ particles prepared at 420 °C in this study.

Because the crystallinity of the sample prepared at 400 °C is better compared with other samples, the samples of high purity, good electrochemical performance in terms of specific capacity and cycling stability can be expected, as shown in Fig. 7. It delivers 120 mA·h/g of specific capacity at the rate of 0.1*C* (see Fig. 7(a)), and maintains about 95% of the initial specific capacity after 50 cycles at the rate of 1*C* (see Fig. 7(b)). On the contrary, the samples prepared at 380 and 390 MPa only deliver 22.1 and 66.9 mA·h/g of specific capacities at the rate of 0.1*C* respectively, indicating that the impurity phases caused by Mn_3O_4 and the serious agglomeration of the particles dramatically decrease the available amount of active $LiMn_2O_4$ particles and restrict the contact between the electrolyte and active $LiMn_2O_4$ particles.

For the sample prepared at 420 °C, the two characteristic voltage plateaus around 4.0 V are not obvious and the specific capacity is much lower than that of the sample prepared at 400 °C. One possible reason is that the lattice of $LiMn_2O_4$ is slightly altered in supercritical water at excessively high reaction

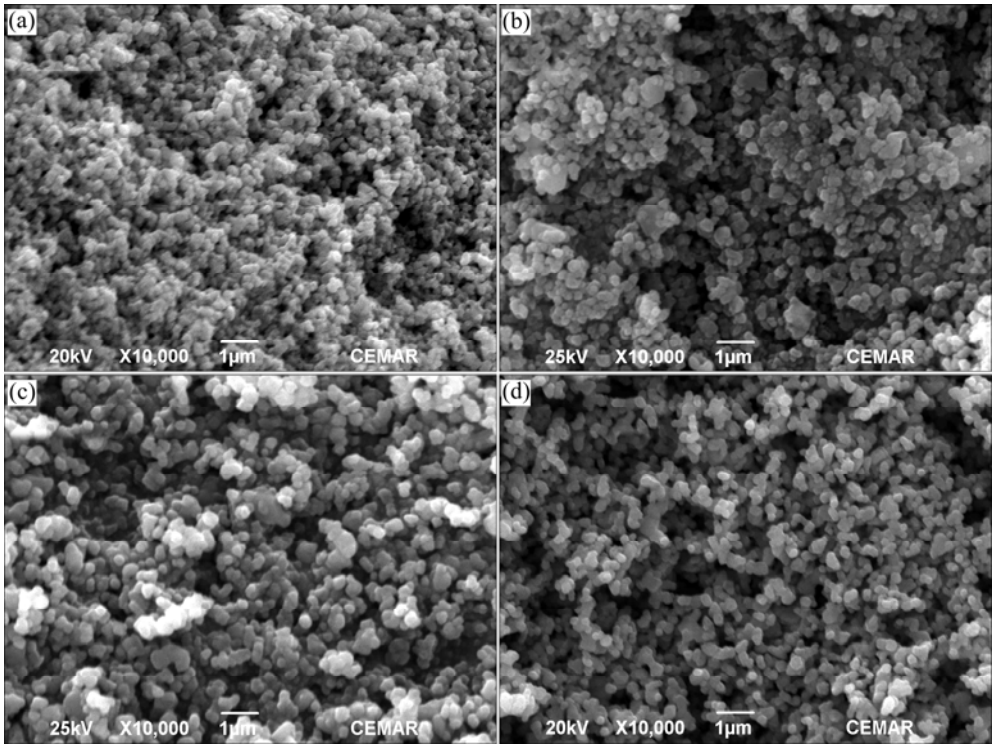

Fig. 6 SEM images of $LiMn_2O_4$ prepared at different SH reaction temperatures: (a) 380 °C; (b) 390 °C; (c) 400 °C; (d) 420 °C

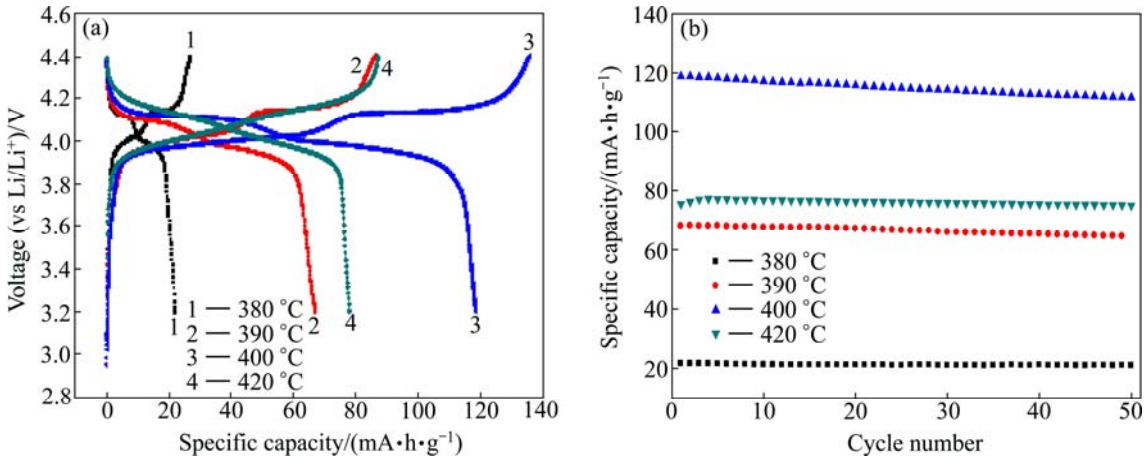

Fig. 7 Discharge−charge profiles at 0.1*C* (a) and cyclic performance at 1*C* (b) of $LiMn_2O_4$ prepared at different SH reaction temperatures

temperature, making the lithium ion more difficult to intercalate/de-intercalate from the Mn−O lattice.

3.3 Effects of SH reaction time on properties of $LiMn_2O_4$ cathode material

Four $LiMn_2O_4$ samples were prepared with SH reaction time of 1, 5, 10 and 15 min, respectively, the SH reaction pressure of 30 MPa and temperature of 400 °C, and followed by SSR at 800 °C for 3 h. Figure 8 presents the XRD patterns of the prepared $LiMn_2O_4$ samples. No impurity peak is found. Moreover, the intensities of the patterns are found to increase when the SH reaction time increases, indicating that the crystallinity of the $LiMn_2O_4$ particles can be improved by lengthening the reaction time appropriately. However, when the SH reaction time increases to 20 min, the resulting powders turn red. They are not lithium manganate apparently with black color. As more Li^+ inserts into the Mn−O structure overtime, the Mn will be oxidized to the valence state of Mn^{4+} under strong alkaline condition. Since an average valence state of $Mn^{3.5+}$ is preferred for $LiMn_2O_4$, 15 min of SH reaction time can be long enough for the proposed $LiMn_2O_4$ preparation route.

The SEM images of $LiMn_2O_4$ prepared with different SH reaction times are shown in Fig. 9. The morphologies of the four $LiMn_2O_4$ samples are similar.

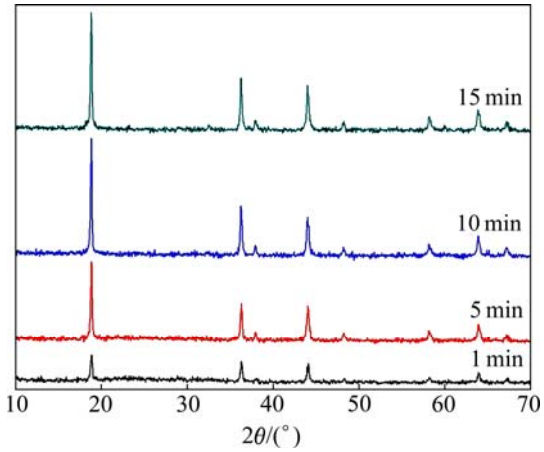

Fig. 8 XRD patterns of samples prepared with different SH reaction time

However, the particle size of the prepared $LiMn_2O_4$ particles increases slightly over the SH reaction time. This phenomenon is reasonable since the particles grow up with longer SH reaction time, which is consistent with XRD results as discussed previously.

The discharge−charge profiles at 0.1*C* and cyclic performance at 1*C* of $LiMn_2O_4$ prepared in different SH reaction times are shown in Fig. 10. The discharge capacity at 0.1*C* for the sample prepared with 15 min of SH reaction time is the highest, namely 123.57 mA·h/g, followed by the samples prepared with 5, 10 and 1 min of SH reaction time with 110.61, 107.00 and 104.48 mA·h/g, respectively. At higher current rate, e.g. 1*C* in this study, these four samples prepared with SH reaction time as 1, 5, 10 and 15 min deliver initial discharge capacities of 103.21, 108.20, 110.86 and

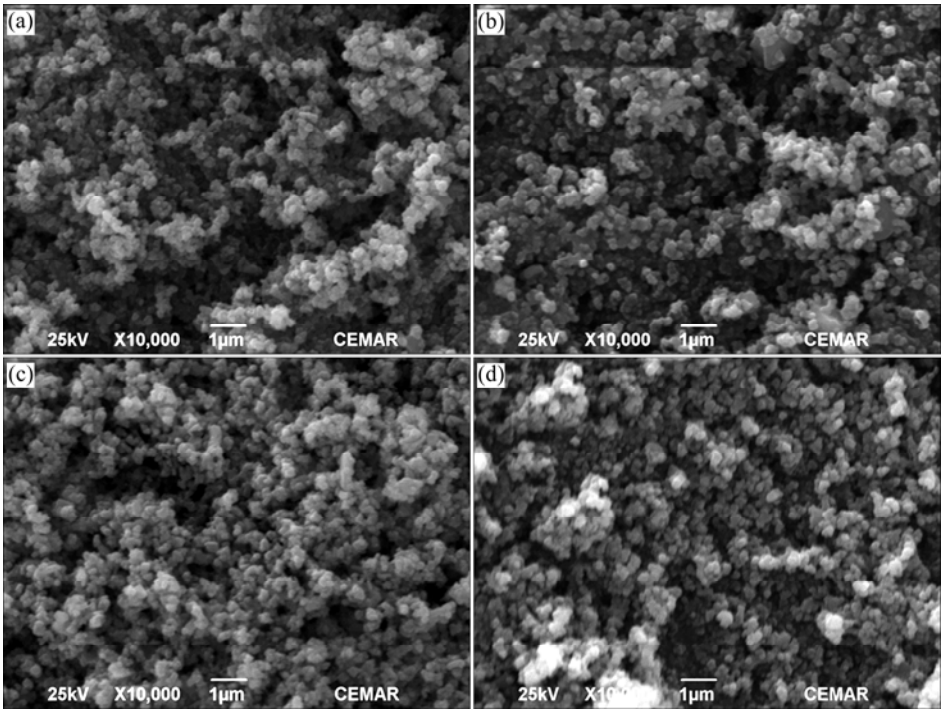

Fig. 9 SEM images of $LiMn_2O_4$ prepared at different SH reaction time: (a) 1 min; (b) 5 min; (c) 10 min; (d) 15 min

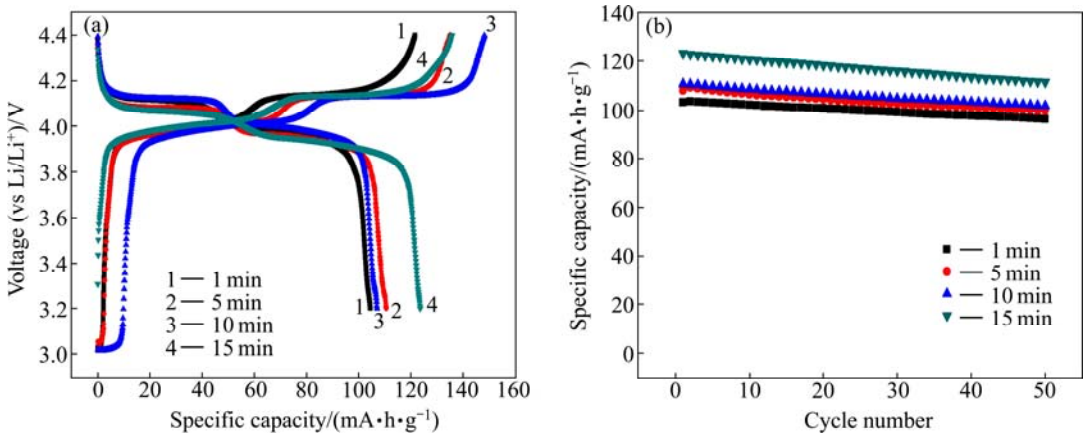

Fig. 10 Discharge−charge profiles at 0.1*C* (a) and cyclic performance at 1*C* (b) of $LiMn_2O_4$ prepared with different SH reaction time

123.29 mA·h/g and capacity retention rates of 93.51%, 92.38%, 91.92% and 90.44% after 50 cycles, respectively. Although the capacity retention rate of the sample prepared with 15 min of SH reaction time is not the highest, it still can deliver a discharge capacity as high as 111.5 mA·h/g after 50 cycles which is higher than the initial capacity of other three samples. As the consequence, a SH reaction time of 15 min is set for the following experiments.

3.4 Effects of SSR reaction temperature on properties of $LiMn_2O_4$ cathode material

In this study, the SSR of spinel $LiMn_2O_4$ cathode material was accelerated by SH route. In order to evaluate the impacts of the reaction temperature of SSR route on the physical and electrochemical properties of $LiMn_2O_4$ cathode material, four samples were prepared by SH route at 400 °C and 30 MPa with 15 min of SH reaction time. One of them was not further treated by SSR route while the rest were sintered at 600, 700 and 800 °C for 3 h, respectively.

The XRD patterns of the as-prepared and calcined $LiMn_2O_4$ cathode materials are shown in Fig. 11. XRD peaks increase as the SSR reaction temperature increases. In addition, the impurity peaks caused by Mn_3O_4 disappear when the SSR reaction temperature is higher than 600 °C. In other words, without heat treatment, the $LiMn_2O_4$ particles prepared by SH route are of poor crystallinity and contain Mn_3O_4 impurity due to the relatively short SH reaction time, i.e. 15 min in this study. The heat treatment provided by SSR route is helpful to improve the crystallinity of $LiMn_2O_4$ particles, and it provides another chance for Mn_3O_4 to react with Li^+ to form spinel $LiMn_2O_4$ particles. However, the SSR reaction temperature is critical for the reaction between Mn_3O_4 and Li^+ for the formation of spinel $LiMn_2O_4$ particles since the SSR reaction time (3 h in this study) is quite short compared with traditional solid state reaction, such as, 72 h at 800 °C as reported by GUYOMARD and TARASCON [5]. As shown in Fig. 11, only when the SSR reaction temperature is higher than 600 °C, the impurity phases caused by Mn_3O_4 disappear. Furthermore, the increase of the SSR reaction temperature is helpful to improve the crystallinity of the spinel $LiMn_2O_4$ as well as its cycling performance and rate performance as discussed later.

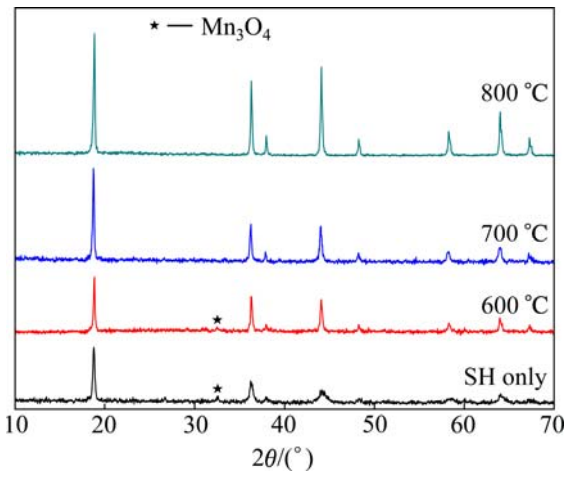

Fig. 11 XRD patterns of samples prepared at different SSR reaction temperatures

The SEM images of these samples are shown in Fig. 12. Compared with the sample prepared by SH route only, the particle size increases after the heat-treatment as well as the crystallinity improves. Moreover, with the increase of the SSR reaction temperature, the morphology of the particles is more likely to be spherical, which is beneficial to improve the cycling performance of the prepared $LiMn_2O_4$ cathode materials.

The electrochemical test results of the prepared $LiMn_2O_4$ without and with heat treatment are shown in Fig. 13, respectively. It is quite interesting that the $LiMn_2O_4$ sample prepared by SH route only delivers 92 mA·h/g of initial specific capacity at a rate of 0.1*C*, while the samples further processed by SSR route at 600, 700 and 800 °C deliver 118, 123 and 120 mA·h/g of initial specific capacity, respectively. The initial specific capacity of the sample prepared at a SSR reaction temperature of 700 °C is larger than the one prepared at 800 °C. However, the cycling stability of the sample prepared at 800 °C is superior to other three samples. It maintained 96.0% of the initial specific capacity after 50 cycles at a rate of 1*C*, while the samples prepared without or with SSR route at 600 and 700 °C only maintain 92.5%, 91.3% and 90.8% of the initial specific capacity, respectively. Moreover, the sample prepared with SSR route at 800 °C delivers 95 mA·h/g of specific capacity, while the samples prepared at 600 and 700 °C of SSR route only deliver 85 and 92.8 mA·h/g at a rate of 50*C*. These results are quite impressed since the excellent rate performance of the spinel $LiMn_2O_4$ cathode material is very essential for its applications in electric vehicles.

3.5 Comparison between commercial and as-prepared $LiMn_2O_4$ cathode materials

As described in the previous sections, the spinel $LiMn_2O_4$ cathode material prepared by SH accelerated SSR route exhibits good crystallinity, uniform size distribution and excellent electrochemical performance. It is therefore interesting to make a comparison between the commercial and as-prepared $LiMn_2O_4$ cathode material in terms of morphology, cycling stability and rate performance. Figures 14 and 15 show the SEM images, cycling stability and rate performance test results of the commercial $LiMn_2O_4$ particles and the $LiMn_2O_4$

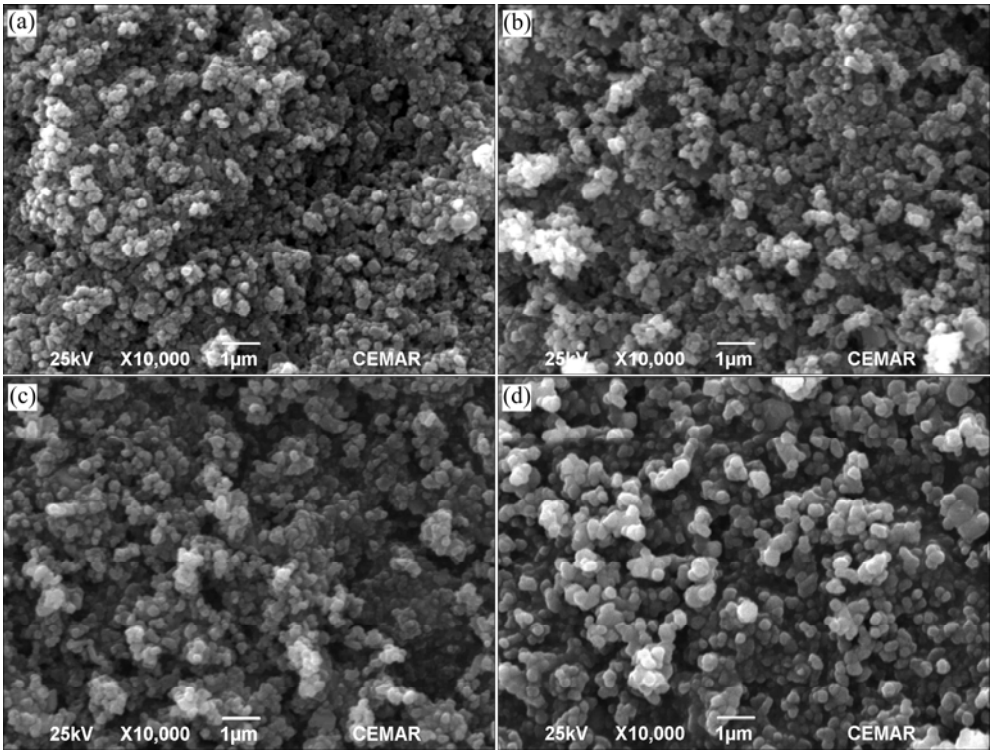

Fig. 12 SEM images of $LiMn_2O_4$ prepared without (a) and with SSR reaction at different temperatures 600 °C (b), 700 °C (c) and 800 °C (d)

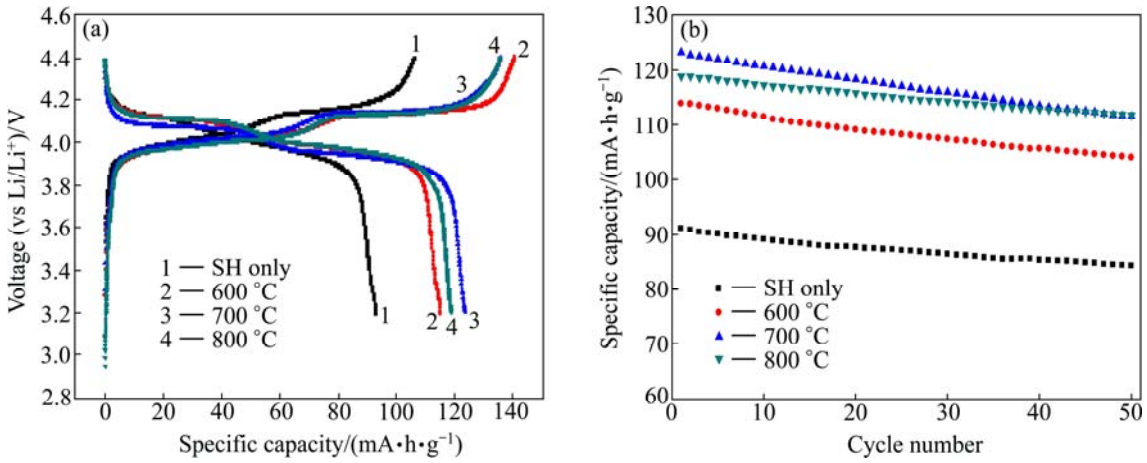

Fig. 13 Discharge−charge profiles at 0.1*C* (a) and cyclic performance at 1*C* (b) of $LiMn_2O_4$ prepared at different SSR reaction temperatures

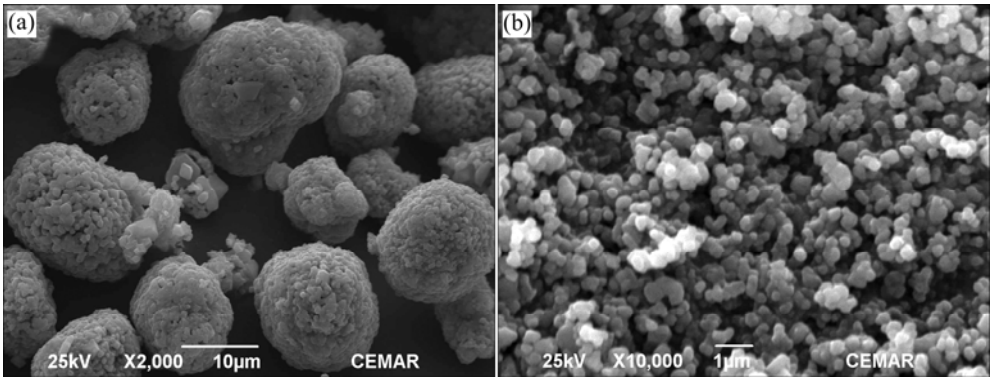

Fig. 14 SEM images of commercial (a) and as-prepared (b) $LiMn_2O_4$ cathode materials

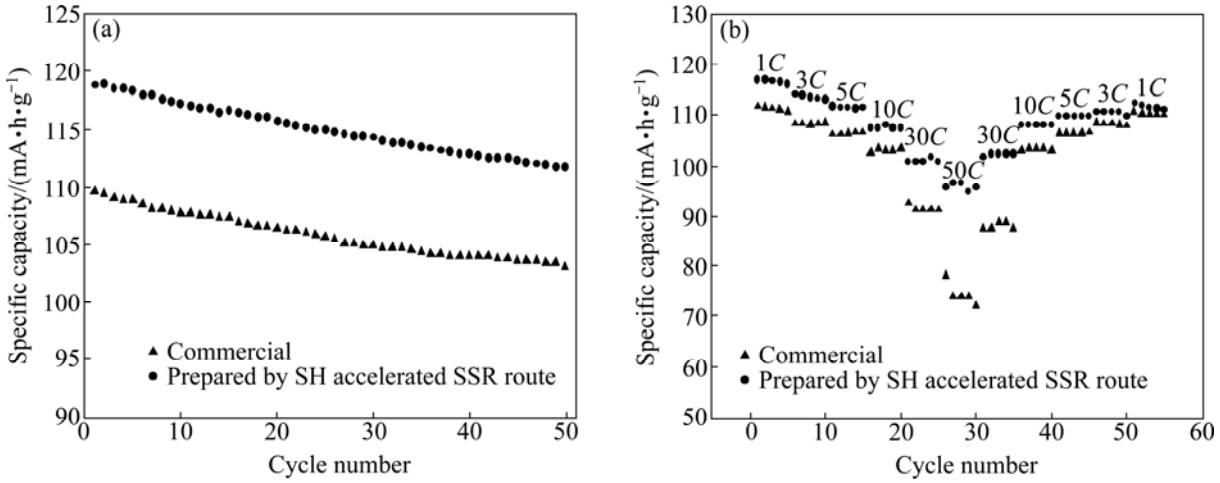

Fig. 15 Electrochemical performance comparisons of commercial and as-prepared $LiMn_2O_4$ cathode material: (a) Cycling stability at 1*C*; (b) Cycling performance at various rates

particles prepared by the proposed SH accelerated SSR route (30 MPa, 400 °C and 15 min SH reaction, 800 °C and 3 h SSR reaction, respectively).

As shown in Fig. 14(a), the commercial $LiMn_2O_4$ products consist of large spherical particles which are agglomerated by nano-sized particles. The size of the commercial $LiMn_2O_4$ spherical particles is about 10 μm. On the contrary, the particle size of the $LiMn_2O_4$ materials prepared by the SH accelerated SSR route is about 300 nm (see Fig. 14(b)). Since the particle size of the $LiMn_2O_4$ material prepared by the SH accelerated SSR route is much smaller than the commercial product, higher specific capacities can be expected, even at high rates. Actually, the nano-structured particles are beneficial to shorten the diffusion distance of Li^+ ions from the electrolyte to the Mn−O lattice in the lithium ion batteries, leading to better electrochemical performance, i.e. specific capacity and cycling stability.

As expected, the prepared samples show superiorities over the commercial samples in the cycling stability and specific capacity at various rates, as shown in Fig. 15. For example, it delivers 118 and 95 mA·h/g of specific capacity at 1 and 50*C*, while the commercial samples only delivers 109 and 70 mA·h/g of specific capacity, respectively. It should be noted that the reaction times of the SH and SSR routes in the proposed method are 15 min and 3 h, respectively, which are much shorter than the one required by the conventional solid state reaction method, i.e. 72 h as reported by GUYOMARD and TARASCON [5]. This can be one of the significant advantages of the proposed SH accelerated SSR route compared with the conventional solid state reaction method since less energy is consumed for the synthesis of the spinel $LiMn_2O_4$ cathode material, especially in the high temperature solid state reaction process.

4 Conclusions

1) Spinel structure $LiMn_2O_4$ cathode materials for Li-ion batteries were successfully synthesized by a supercritical-hydrothermal accelerated solid state reaction route.

2) The experimental results showed that the reaction pressure, reaction temperature and reaction time of SH route and SSR reaction temperature have significant impacts on the physical and electrochemical performance of the $LiMn_2O_4$ cathode materials. It is found that the samples prepared with 30 MPa, 400 °C, 15 min SH route and 800 °C, 3 h SSR reaction are better than the samples prepared with other experimental conditions considered in terms of particle crystallinity, size distribution and electrochemical properties. Specially, they deliver 120 mA·h/g of specific capacity at 0.1*C*, and maintain over 96.0% of the initial specific capacity after 50 cycles at 1*C*. Moreover, their specific capacity could reach 95 mA·h/g even at 50*C* rate, which is very promising for their applications in electric vehicles.

References

[1] JEFFREY W F. Recent developments in cathode materials for lithium ion batteries [J]. Journal of Power Sources, 2010, 195(4): 939−954.

[2] MICHAEL M T. Manganese oxides for lithium batteries [J]. Progress in Solid State Chemistry, 1997, 25(1−2): 1−71.

[3] ALCANTARA R, LAVELA P, RELANO P L, TIRADO J L. X-ray diffraction, EPR, and ^{6}Li and ^{27}Al MAS NMR study of $LiAlO_2$−$LiCoO_2$ solid solutions [J]. Inorganic Chemistry, 1998, 37(2): 264−269.

[4] HUNTER J C. Preparation of a new crystal form of manganese dioxide: Lambda-MnO_2 [J]. Solid State Chemistry, 2009, 39(2): 142−147.

[5] GUYOMARD D, TARASCON J M. Rechargeable $Li_{1+x}Mn_2O_4$/carbon cells with a new electrolyte composition [J]. Journal of Electrochemistry Society, 1993, 140: 3071−3081.

[6] WAN Chuan-yun, MIN Cheng, DI Wu. Synthesis of spherical spinel $LiMn_2O_4$ with commercial manganese carbonate [J]. Powder Technology, 2011, 210(1): 47−51.

[7] LIU X M, HUANG Z D, OH S, MA P C, CHAN P C, VEDAM G K, KANG K, KIM J K. Sol–gel synthesis of multiwalled carbon nanotube-$LiMn_2O_4$ nanocomposites as cathode materials for Li-ion batteries [J]. Journal of Power Sources, 2010, 195(13): 4290−4296.

[8] YAN Hong-wei, HUANG Xue-jie, CHEN Li-quan. Microwave synthesis of $LiMn_2O_4$ cathode material [J]. Journal of Power Sources, 1999, 81−82: 647−650.

[9] DU K, HU G R, PENG Z D, QI L. Synthesis of spinel $LiMn_2O_4$ with manganese carbonate prepared by micro-emulsion method [J]. Electrochimica Acta, 2010, 55(5): 1733−1739.

[10] KARTHICK S N, RICHARD PRABHU GNANAKAN S, SUBRAMANIA A, KIM H J. Nanocrystalline $LiMn_2O_4$ thin film cathode material prepared by polymer spray pyrolysis method for Li-ion battery [J]. Journal of Alloys and Compounds, 2010, 489(2), 674−677.

[11] PARK K C, WANG F, MORIMOTO S, FUJISHIGE M, MORISAKO A, LIU X X, KIM Y J, JUNG Y C, JANG I Y, ENDO M. One-pot synthesis of iron oxide–carbon core–shell particles in supercritical water [J]. Materials Research Bulletin, 2009, 44: 1443−1450.

[12] LEE J W, LEE C H. Synthesis of Zn_2SnO_4 anode material by using supercritical water in a batch reactor [J]. Journal of Supercritical Fluids, 2010, 55(1): 252−258.

[13] LIU Xue-wu, WEI Hao, DENG Yuan-fu, TANG Jie, SHI Zhi-cong, CHEN Guo-hua. Synthesis of sub-micrometer lithium iron phosphate particles using supercritical hydrothermal method for lithium ion batteries [J]. Journal of Shanghai Jiao Tong University, 2012, 17(5): 1−6.

[14] HONG S A, Kim S J, KIM J, LEE B G, CHUNG K Y, LEE Y W. Carbon coating on lithium iron phosphate ($LiFePO_4$): Comparison between continuous supercritical hydrothermal method and solid-state method [J]. Chemical Engineering Journal, 2012, 189−199: 318−326.

[15] KANAMURA K, DOKKO K, KAIZAWA T. Synthesis of spinel $LiMn_2O_4$ by a hydrothermal process in supercritical water with heat-treatment [J]. Journal of the Electrochemical Society, 2005, 152(2): A391−A395.

[16] NUGROHO A, KIM S J, CHUNG K Y, CHO B W, LEE Y W, KIM J. Facile synthesis of nanosized $Li_4Ti_5O_{12}$ in supercritical water [J]. Electrochemistry Communications, 2011, 13: 650−653.

超临界水热合成结合固相煅烧制备高性能锂离子电池的锰酸锂正极材料

刘学武[1,2]，汤 洁[1]，覃旭松[2]，邓远富[3]，陈国华[2,4]

1. 大连理工大学 化工机械学院，大连 116024；
2. 广州市香港科大霍英东研究院 绿色产品及加工技术研究中心，广州 511458；
3. 华南理工大学 化学与化工学院，广州 510640；
4. 香港科技大学 化学工程及生物分子工程学系，香港

摘 要：采用超临界水热合成与高温固相合成相结合的方法制备亚微米级锂离子电池锰酸锂正极材料，研究超临界水热合成过程中的反应压力、反应温度、反应时间和高温固相合成过程中煅烧温度对合成材料的纯度、形貌及电化学特性的影响。结果表明：相对于传统的高温固相合成方法，在 400 °C 和 30 MPa 的条件下，经过 15 min 超临界水热反应获得的 $LiMn_2O_4$ 电池材料，在后续 800 °C 煅烧温度下的煅烧时间可缩短到 3 h。在该条件下合成的 $LiMn_2O_4$ 正极材料具有良好的结晶度、均匀的粒度分布和优异的电化学性能，在 0.1*C* 下的首次放电比容量达到 120 mA·h/g，且在 50*C* 的高倍率下仍然表现出良好的放电性能。

关键词：锂离子电池；锰酸锂；超临界水；固相反应；高倍率性能

(Edited by Chao WANG)